Available online at www.sciencedirect.com
ScienceDirect
International Journal of Heat and Mass Transfer 51 (2008) 302–311
International Journal of HEAT and MASS TRANSFER
www.elsevier.com/locate/ijhmt

On predicting two-dimensional heat transfer in a cylindrical porous media combustor

Nelson O. Moraga [a,*], César E. Rosas [a], Valeri I. Bubnovich [b], Nicola A. Solari [a]

[a] Mechanical Engineering Department, Universidad de Santiago de Chile, Alameda 3363, Santiago, Chile
[b] Chemical Engineering Department, Universidad de Santiago de Chile, Alameda 3363, Santiago, Chile

Received 3 November 2006; received in revised form 30 March 2007
Available online 8 June 2007

Abstract

Convective heat transfer within a cylindrical inert porous media combustor is studied. A two-dimensional, two temperature mathematical model, based on fluid mechanics, energy and chemical species governing equations is used for combustion simulation. The finite volume method is used to solve the discrete model for methane combustion with air. Results are presented for unsteady velocity and temperature distributions, as well as for the displacement of the combustion zone, to assess the effects of inlet reactants velocities in the range 0.3–0.6 m/s; excess air ratios between 3 and 6 and porosities of 0.3 up to 0.6 in the convection heat transfer and combustion processes.

Keywords: 2D heat transfer; Cylindrical porous combustor; Finite volume simulation

1. Introduction

Combustion in porous media offers a variable dynamic power range, high power density and very low emissions of CO and NO_x [1]. Burners based on this technology has been built and tested for many applications. Household burners for air and warm water heating systems, porous medium combustors combined with pre-mixed industrial burners, air heating systems for dryers, gas turbine combustion chambers, heating systems and pre-heaters for cars, burners for steam generation have been described by Trimis and Durst [2] and Möβbauer et al. [1].

Most of the studies developed in this area previous to one decade ago used 1D models to analyse theoretical and numerically the combustion in porous media. Analytical expressions predicting the combustion wave velocity and temperature distributions for a diluted methane–air combustion in a porous media have been found in qualitative agreement with experimental results [3]. Experimental studies for lean methane–air mixtures, under stable combustion conditions over a wide range of air/fuel ratios, $11 < A/F < 60$ were reported by Zhdanok et al. [4]. They developed one analytical prediction of the dimensionless wave velocity that was in good agreement with their own experimental results, and with those values measured for hydrogen-fuel-rich mixtures by Babkin [5]. Experimental measurements on reaction rates, flammability limits and flame stabilization in combustion within porous media, along with modeling and prediction of flame speeds, temperature and concentration profiles and radiative efficiency have been reviewed by Howell et al. [6]. The flame front localization inside axis-symmetric cylindrical and spherical porous media burners have been found analytically and numerically to depend on heat losses, fuel flow rate, heat content of the mixture and on the external radius [7].

A detailed chemistry in the modeling has been found to be important for near stoichiometric and rich flames, but is less important for very lean flames [8]. The GRI 1.2 chemical kinetic mechanism, in which 32 species are participating in 177 elementary reactions, has been used to predict

* Corresponding author. Tel.: +56 2 718 3005; fax: +56 2 682 5498.
E-mail address: nmoraga@lauca.usach.cl (N.O. Moraga).

0017-9310/$ - see front matter © 2007 Elsevier Ltd. All rights reserved.
doi:10.1016/j.ijheatmasstransfer.2007.03.041

Nomenclature

C_p	specific heat (J/kg K)
D^M	diffusion coefficient (m^2/s)
dp	pore diameter (m)
E_a	activation energy (J/mol)
h	heat transfer coefficient to the outside (W/m^2 K)
h_{RAD}	heat transfer coefficient to the outside by radiation (W/m^2 K)
K	frequency factor (1/s)
Pr	Prandtl number
Nu	Nusselt number
R_0	universal gas constant (J/mol K)
T	temperature (K)
t	time (s)
u_G	speed of gases (m/s)
u_{inst}	interstitial speed of gases (m/s)
w_f	fuel mass fraction

Greek symbols

Δh	combustion enthalpy (J/kg)
α	superficial heat interchange coefficient between gas and solid (W/m^3 K)
λ	thermal conductivity (W/m K)
ε	porosity
ε'	porous media emissivity
μ	dynamic viscosity of gas (kg/m s)
ρ	density (kg/m^3)
σ	Stephan–Boltzmann constant ($W/m^2 K^4$)
τ	quartz transmissivity
ψ	excess of air

Subscripts

0	initial condition
eff	effective
G	gas
S	solid

methane combustion in porous media by Henneke and Ellzey [9]. The results obtained by Zhdanok et al. [4], from a one-dimensional model, for solid temperature were found to be in good agreement with previous experimental data, when the equivalence ratio was equal to 0.15.

Temperatures and concentrations of CO and NO of a lean pre-mixed methane–air mixture on ceramic foam burners are predicted well with one-dimensional models, that have been solved by using different numerical methods based on finite differences or by finite volume methods [10].

The internal heat recirculation in a honeycomb ceramic combustor, investigated experimentally and theoretically, extended the ranges of flammability and flame stability [11]. The presence of one stable mode and a push-forward combustion mode has been observed in experiments to assess some effects of preheating conditions of a propane/air mixture on combustion in a stack of stainless steel screens [12]. Flame stabilization in a two section porous burner for methane/air mixtures, with 0.55–0.80 equivalence ratios, has been numerically studied by Barra et al. [13]. The results obtained show that the upstream section should have low of conductivity and volumetric heat transfer coefficient and high radiative extinction coefficient and the downstream section should have high conductivity, high volumetric heat transfer coefficient and an intermediate radiative extinction coefficient.

In the last decade some studies using 2D mathematical models has been developed in order to have better simulations and capture physical effects that can not be accomplished based on a 1D model. Two types of two-dimensional effects have been reported in the literature. The first one is the non-uniform radial temperature distribution due to the high wall heat looses in combustors of small diameters. Calculations from two-dimensional models performed for a porous medium burner with a rectangular cross-section geometry have been found to be in good agreement with experimental results [14,15]. The second effect is the theoretical prediction of two-dimensional hydrodynamic instability leading to the inclination of the combustion wave experimentally noticed in combustors of large diameters [16], which is an obstacle to use porous media burners in industry. Dobrego et al. [17] studied theoretically, numerically and experimentally the combustion wave inclination instability. They found that inclination amplitude growth velocity on the linear stage is a function of combustion wave velocity, the combustor diameter and of the diameter of the porous media particles.

Taking in account the state of art on combustion in porous media and its potential applications in household and industrial burners, this paper studies the heat transfer and fluid mechanics in a cylindrical porous media burner, where a combustion process of methane/air mixture takes place, in order to provide tools of analysis to optimize the location of the heat exchanger devices. The study is developed by means of a two-dimensional, two temperature equations mathematical model, built based on continuity, linear momentum, energy and fuel fraction mass partial differential equations to predict the effect of the basic parameters on the convective heat transfer in the inert porous media combustor. The finite volume method is used to solve the highly non-linear mathematical model and to assess the effects of porosity, inlet air velocity and excess of air.

2. Physical situation and mathematical model

The physical situation of a porous media combustor, built on base of alumina spheres placed inside of a axis-symmetric cylindrical quartz tube of 0.52 m in length and 0.076 m in diameter, is shown in Fig. 1. Methane and air mixture enter to the combustor at ambient temperature with uniform velocity. To start the combustion a temperature profile of one step type, with a maximum temperature of 1150 K and a thickness of 4 cm is assumed to simulate the ignition by means of an external energy source. In the combustion zone, the products: CO_2, H_2O, O_2 and N_2 are generated. Air, gas and products are assumed to behave as ideal gases and hence density is calculated in terms of temperature from the ideal gas state equation. The pressure drop of the flow through the channel is neglected.

The mathematical model is built on base of the following assumptions: A single-step chemical reaction, laminar 2D flow of Newtonian and incompressible fluid.

The governing equations are:

A single step chemical reaction

$$CH_4 + 2(1+\psi)(O_2 + 3.76N_2) \rightarrow CO_2 + 2\cdot H_2O + 2\psi\cdot O_2 + 7.52(1+\psi)N_2 \quad (1)$$

Continuity equation

$$\frac{\partial(\rho v_r)}{\partial r} + \frac{\rho v_r}{r} + \frac{\partial(\rho v_z)}{\partial z} = 0 \quad (2)$$

Linear momentum equation.

In the present study this equation is used in an approximate form, as in most of the works developed by others authors [14,15], because for the range of physical parameters used in the calculations the effects of the porous media on the fluid flow, the complete Darcy, Brinkman and Forchheimer model is not required. This consideration is taken in based on the facts that the solution of a more complex model requires major computational effort.

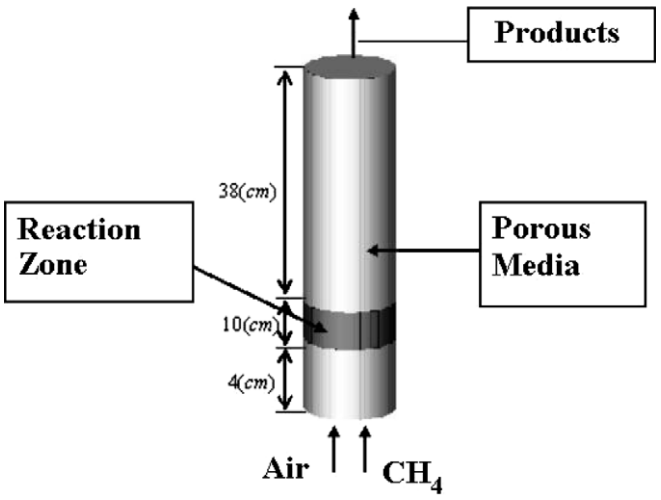

Fig. 1. Physical situation of porous media burner.

Linear momentum in r

$$\rho\left(\frac{\partial v_r}{\partial t} + v_r\frac{\partial v_r}{\partial r} + v_z\frac{\partial v_r}{\partial z}\right) = -\frac{\partial p}{\partial r} + \mu\left(\frac{\partial^2 v_r}{\partial r^2} + \frac{1}{r}\frac{\partial v_r}{\partial r} - \frac{v}{r^2} + \frac{\partial^2 v_r}{\partial z^2}\right) \quad (3)$$

Linear momentum in z

$$\rho\left(\frac{\partial v_z}{\partial t} + v_r\frac{\partial v_z}{\partial r} + v_z\frac{\partial v_z}{\partial z}\right) = -\frac{\partial p}{\partial z} + \mu\left(\frac{\partial^2 v_z}{\partial r^2} + \frac{1}{r}\frac{\partial v_z}{\partial r} + \frac{\partial^2 v_z}{\partial z^2}\right) \quad (4)$$

Mass conservation equation for fuel vapor

$$\rho\left(\frac{\partial w}{\partial t} + v_r\frac{\partial w}{\partial r} + v_z\frac{\partial w}{\partial z}\right) = \frac{\partial}{\partial r}\left(D^{\mathrm{M}}\cdot\rho\cdot\frac{\partial w}{\partial r}\right) + \frac{\partial}{\partial z}\left(D^{\mathrm{M}}\cdot\rho\cdot\frac{\partial w}{\partial z}\right) - \rho\cdot K\cdot w\cdot e^{\frac{-E_a}{R_0\cdot T}} \quad (5)$$

Energy equation for gas in porous media

$$\varepsilon(\rho\cdot C_p)\left(\frac{\partial T_G}{\partial t} + v_r\frac{\partial T_G}{\partial r} + v_z\frac{\partial T_G}{\partial z}\right) = -\alpha(T_G - T_S) - \varepsilon\cdot\rho\cdot\Delta h\cdot K\cdot w\cdot e^{\frac{-E_a}{R_0\cdot T}} \quad (6)$$

Energy equation for solid in porous media

$$(1-\varepsilon)(\rho\cdot C_p)_S\left(\frac{\partial T_S}{\partial t}\right) = \frac{1}{r}\frac{\partial}{\partial r}\left(r\cdot\lambda_{\mathrm{eff}}\frac{\partial T_S}{\partial r}\right) + \frac{\partial}{\partial z}\left(\lambda_{\mathrm{eff}}\frac{\partial T_S}{\partial z}\right) + \alpha(T_G - T_S) \quad (7)$$

Ideal gas state equation

$$\rho = \frac{\rho_0\cdot T_0}{T} \quad (8)$$

The initial conditions are inlet uniform temperature and velocity for the reactants

$$T_0 = 300\ \mathrm{K} \quad (9)$$

$$w_f = \frac{1}{1 + 17.16\cdot(1+\psi)} \quad (10)$$

Boundary conditions in the tube wall

$$\lambda_{\mathrm{eff}}\frac{\partial T_S}{\partial x} = (h + h_{\mathrm{RAD}})\cdot(T_S - T_0) \quad (11)$$

$$h_{\mathrm{RAD}} = \varepsilon'\cdot\tau\cdot\sigma\cdot(T_S - T_0)\cdot(T_S^2 - T_0^2) \quad (12)$$

$$\lambda_G\frac{\partial T_G}{\partial x} = h\cdot(T_G - T_0) \quad (13)$$

and developed flow conditions at the outlet

$$\frac{\partial T_S}{\partial x} = \frac{\partial T_G}{\partial x} = \frac{\partial w}{\partial x} = 0 \quad (14)$$

The properties used in the numerical simulations are presented in Table 1.

The mass diffusion coefficient was found by assuming that the Lewis number was equal to 1,

Table 1
Properties of gas and solid

Alumine	Gas
$\rho_S = 4100\ \text{kg/m}^3$	$C_{p_G} = 947\ e^{0.00183 \cdot T}\ \text{J/kg K}$
$C_{p_S} = 92.688 \cdot T^{0.3797}\ \text{J/kg K}$	$\mu_G = 3.37\text{E}{-7} \cdot T^{0.7}\ \text{kg/m s}$
$\lambda_{eff} = \lambda_S(1-\varepsilon) + \lambda_{RAD}$	
$\lambda_S = 2.17\ \text{W/m K}$	
$\lambda_{RAD} = \frac{32 \cdot \sigma \cdot \varepsilon \cdot dp \cdot T^3}{9 \cdot (1-\varepsilon)}$	

$$D^M = \frac{\lambda_G}{(\rho \cdot C_p)_G} \quad (Le = 1) \tag{15}$$

$$\lambda_G = \frac{\mu \cdot C_p}{Pr} \tag{16}$$

The coefficient of convective heat transfer between solid and gas are:

$$\alpha = 6 \cdot (1-\varepsilon) \cdot \lambda_G \cdot \frac{Nu}{dp^2} \tag{17}$$

$$Nu = 2 + 1.1 \cdot Pr^{\frac{1}{3}} \cdot Re^{0.6} \tag{18}$$

$$Re = \rho \cdot u_0 \cdot \varepsilon \cdot \frac{dp}{\mu} \tag{19}$$

$$\lambda_G = \frac{\mu \cdot C_p}{Pr} \tag{20}$$

Additional parameters used in the simulation were the Stephan–Boltzmann constant (σ), combustion enthalpy (Δh), frequency factor (K), activation energy (E_a) and universal gas constant (R_0).

$$\sigma = 5.67 \times 10^8\ \text{W/m}^2\ \text{K}^4; \quad \Delta h = 50.15 \times 10^6\ \text{J/kg} \tag{21}$$

$$K = 2.6 \times 10^8\ (1/\text{s}); \quad E_a/R_0 = 15643.8\ \text{K} \tag{22}$$

3. Solution procedure

The coupled, strongly non-linear system of equations was solved by using the finite volume method, along with the SIMPLE algorithm, Patankar [18]. A fifth power law was used to calculate the convective terms while the difussion terms were determinated by linear interpolation functions for the dependent variables between the nodes.

Each one of the governing equations was written in the general form of the transport equation, with unsteady, convective, diffusion and linearized source terms

$$\frac{\partial(\rho \cdot \phi)}{\partial t} + \text{div}(\rho \cdot \vec{v} \cdot \phi) = \text{div}(\Gamma \cdot \text{grad}\phi) + Sc + Sp \cdot \phi \tag{23}$$

The diffusion coefficient (Γ) and the source terms (Sc, Sp) for each dependent ϕ variable are presented in Table 2.

The convergence criteria used for gas and solid temperature and for fuel mass fraction were

$$|\phi_{i,j}^k - \phi_{i,j}^{k-1}| \leqslant 10^{-3} \tag{24}$$

while for the two velocity components a more restrictive criteria was imposed

Table 2
Diffusion coefficient and source terms for the 2D model

ϕ	Γ	S_C	S_P
u	$\frac{\mu_G}{\rho_G}$	$\frac{u_{(ant)}}{\Delta t}$	$-\frac{1}{\Delta t}$
v	$\frac{\mu_G}{\rho_G}$	$\frac{v_{(ant)}}{\Delta t}$	$-\frac{1}{\Delta t}$
T_G	$\frac{\mu_G}{(\rho \cdot Pr)_G}$	$\left(\frac{\Delta h \cdot r_f}{(\rho C_P)_G} + \frac{\alpha T_S}{(\rho C_P)_G} + \frac{T_{G(ant)}}{\Delta t}\right)$	$-\left(\frac{\alpha}{(\rho C_P)_G} + \frac{1}{\Delta t}\right)$
w_i	$\frac{\mu_G}{(\rho \cdot Pr)_G}$	$\frac{w_{i(ant)}}{\Delta t}$	$-\left(\frac{K \cdot \exp\left(-\frac{E_a}{R_0 \cdot T}\right)}{(C_P)_G} + \frac{1}{\Delta t}\right)$
T_S	λ_{eff}	$\left(\alpha T_G + \beta T + \frac{T_{S(ant)}(\rho C_p)_S}{\Delta t}\right)$	$-\left(\alpha + \beta + \frac{(\rho C_p)_S}{\Delta t}\right)$

Table 3
Time steps used in the simulation

Time (s)	Time steps, Δt (s)
$t < 0.001$	$\Delta t = 0.00001$
$0.001 < t < 0.01$	$\Delta t = 0.0001$
$0.01 < t < 0.1$	$\Delta t = 0.001$
$t > 0.1$	$\Delta t = 0.1$

$$|\phi_{i,j}^k - \phi_{i,j}^{k-1}| \leqslant 10^{-4} \tag{25}$$

A non-uniform grid of 622×15 nodes was found, by a trial and error procedure to be efficient in order to solve the problem with accuracy and reasonable computation time.

The iterative calculation procedure was based in the line by line method, that combines the Thomas algorithm (TDMA) with the under – relaxed Gauss – Seidel algorithm. The under relaxation coefficients used were equal to 0.1 for the u and v velocity components, and 0.5 for gas and solid temperature and for the fuel fraction.

A strategy based on the use of a dynamic time step was implemented and the different values of the time steps used in the unsteady calculations are presented in Table 3.

4. Results and discussion

Numerical experiments were performed to assess the effect of porosity, inlet gas velocity and coefficient of excess of air changes on the fluid mechanics and heat transfer in the porous matrix combustor. Most of the reported results were calculated for a porous media with $\varepsilon = 0.4$. Some calculations are reported for porosities of 0.3 and 0.6, that can be obtained by a homogeneous mixture of spherical particles of different diameters.

The effect of a change in the porosity of the porous matrix, from $\varepsilon = 0.3$ to $\varepsilon = 0.6$ on the axial component of the velocity is shown in Fig. 2, at four axial locations of the combustor: 0.05 m, 0.1 m, 0.15 m and 0.21 m. The axial velocity profile is shown, for each location, at times equal to 300, 600, 900, 1200 and 1500 s. The increment of the porosity from $\varepsilon = 0.3$ to $\varepsilon = 0.6$ shows a reduction in the axial velocity component and in the velocity gradients at the combustor wall. The transient change of the velocity, caused by density changes due to the porous media heating

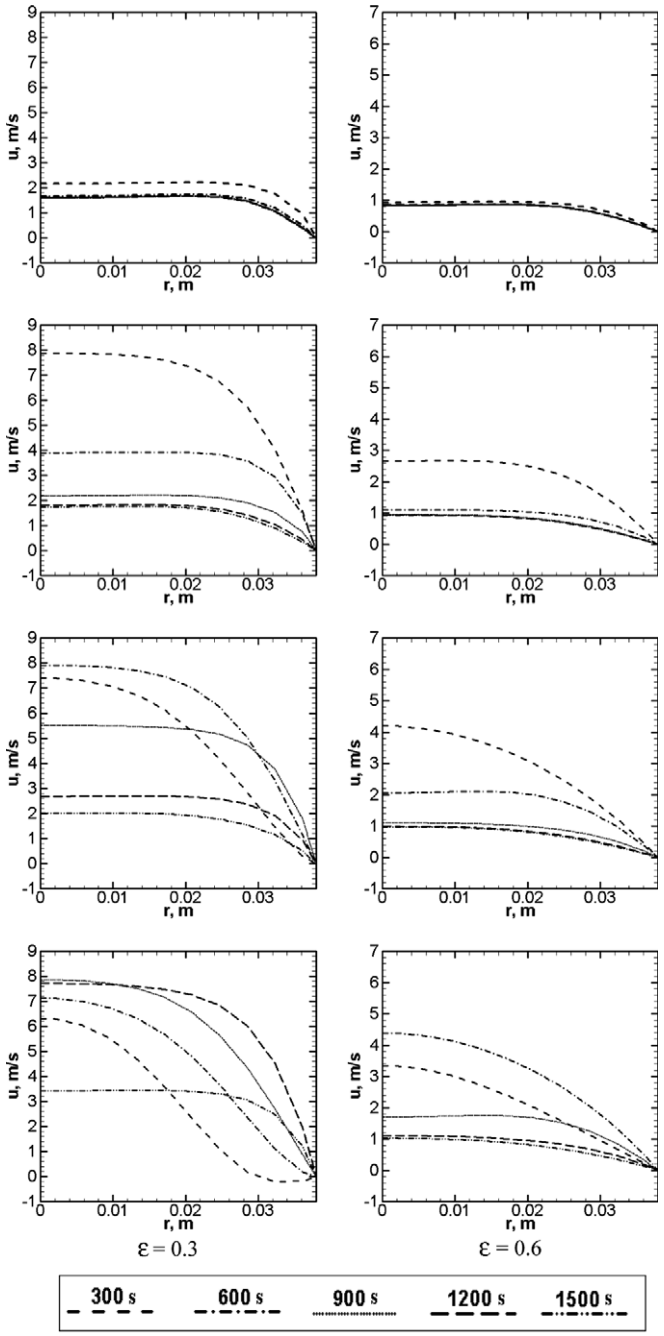

Fig. 2. Effect of porosity on the axial velocity along the burner. Axial locations (from top to the bottom): 0.05 m, 0.10 m, 0.15 m and 0.21 m. $U_0 = 0.43$ m/s, $\psi = 4.88$. Left side $\varepsilon = 0.3$; Right side $\varepsilon = 0.6$.

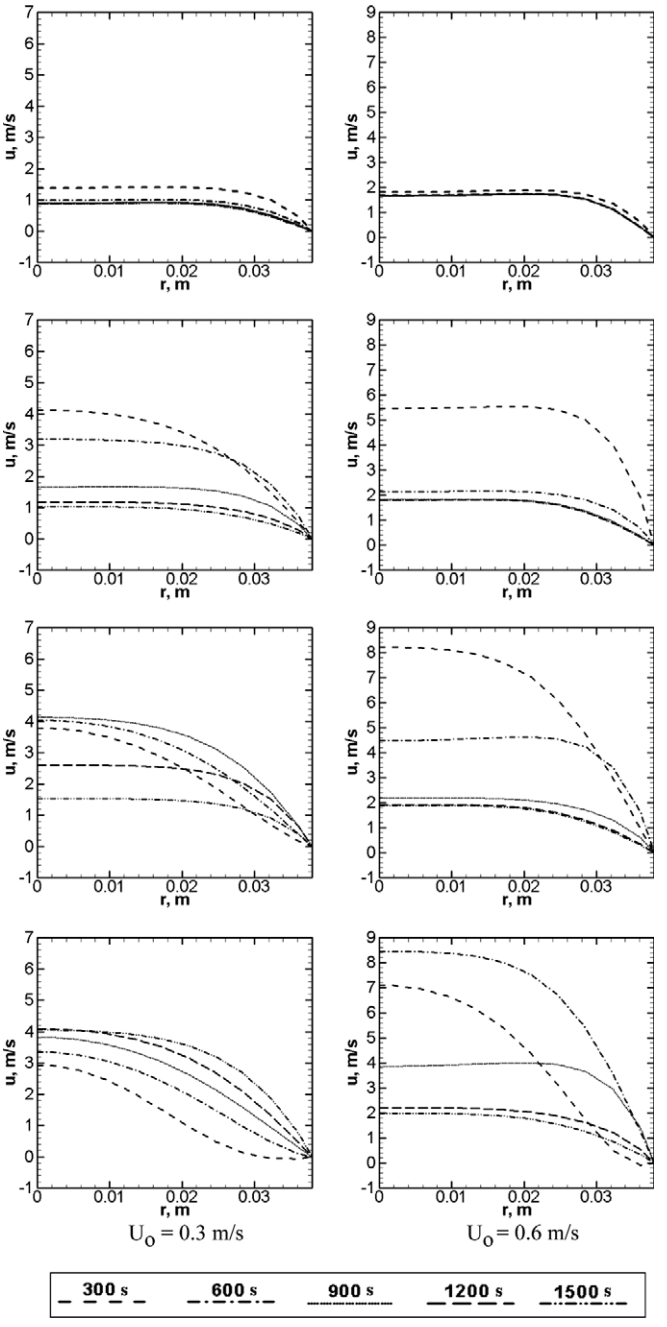

Fig. 3. Effect of the inlet velocity on the axial velocity along the burner. Axial locations (from top to the bottom): 0.05 m, 0.10 m, 0.15 m and 0.21 m. $\psi = 4.88$, $\varepsilon = 0.4$. Left side: $U_0 = 0.30$ m/s; right side: $U_0 = 0.60$ m/s.

process, are negligible at a distance of 0.05 m from the inlet. The axial velocity profile is observed to increase with time, with a maximum velocity profile, reached when $t = 600$ s at a distance equal to 0.15 m from the inlet when $\varepsilon = 0.3$ and, at $z = 0.21$ m when $\varepsilon = 0.6$. Secondary flows are developed near the combustor wall when $\varepsilon = 0.3$ at $z = 0.21$ m, after 300 s of initiating the combustion. After the combustion front has crossed the zone at $z = 0.21$ m, the secondary flows are seen to disappear.

Fig. 3 shows the influence of the inlet velocity in the unsteady axial velocity profile for a combustor with a porosity value equal to 0.4. Unsteady changes in the axial velocity profiles are seen to be larger when the inlet velocity is 0.6 m/s. When the inlet axial velocity of air and methane is equal to 0.3 m/s, the axial velocity profile increases with time, until maximum values are found at 900 s for an axial location of 0.15 m and up to 1500 s, for the region located at $z = 0.21$ m.

The temperature in the porous media combustor varies from 300 K near the inlet and close to the outlet to approximately 1600 K in the flame region. Calculated temperature

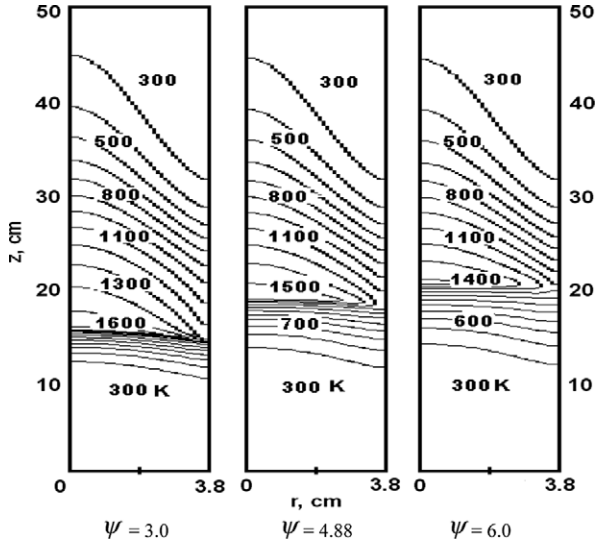

Fig. 4. Effect of the excess of air on the gas temperature at a time equal to 15 min, for $U_0 = 0.43$ m/s; $\varepsilon = 0.4$. Excess of air $\psi = 3.0$ (left side); 4.88 (center); 6.0 (right side).

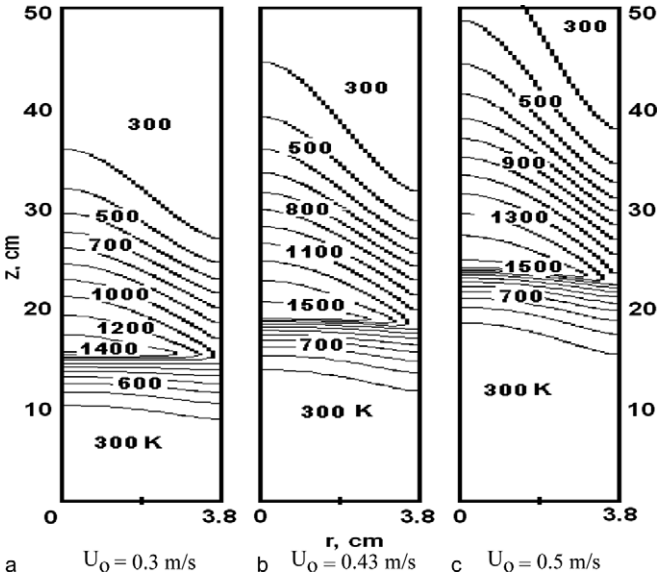

Fig. 6. Gas temperature at $t = 15$ min, $\varepsilon = 0.4$ and $\psi = 3.0$ for inlet velocities $U_0 = 0.3$, 0.43 and 0.5 m/s.

distributions for the porous combustor are depicted at Figs. 4–6. An increment of the air excess ratio ψ from 3.0 to 4.88 and up to $\psi = 6.0$ reveals that at the burning time equals to 15 min lower temperatures are obtained near the flame region and a displacement of the combustion region toward the middle of the combustor is achieved. Similar effects in the temperature distribution in the porous combustor can be noticed in Fig. 5 when the porosity is changed from $\varepsilon = 0.3$ to $\varepsilon = 0.6$. A large uniform temperature region at the inlet temperature, that is located in one third of the initial region of the combustor is observed at a burning time of 15 min when the porosity of the combustor $\varepsilon = 0.6$. The displacement of the combustion zone in the direction of the burner exit is strongly influenced by the increments in the values of the three parameters: excess air ratio, porosity and inlet reactants velocity, as it can be noticed by inspecting Figs. 4–6, and Table 4. The results obtained show that the displacement velocity of the combustion front increases with the porosity and inlet reactants velocity, and decreases with the excess air ratio.

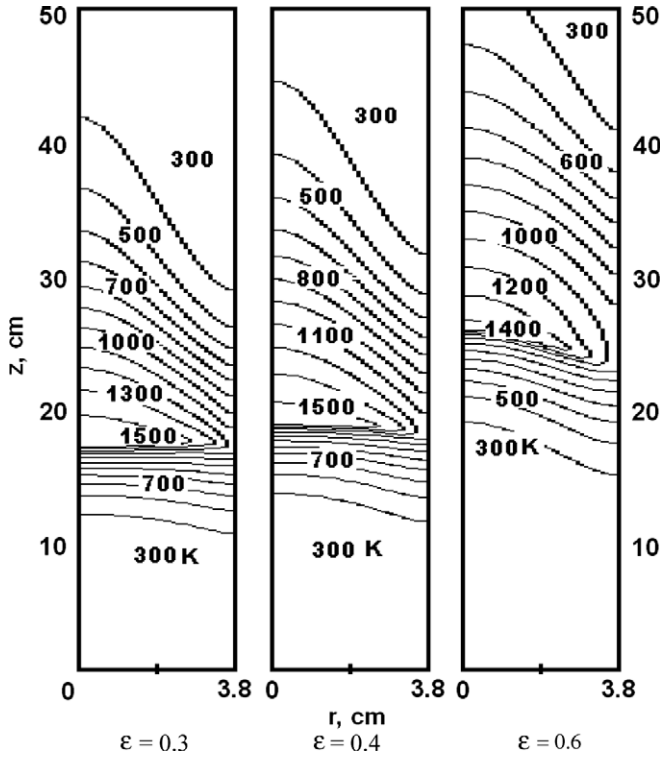

Fig. 5. Influence of porosity on gas temperature at a time equal to 15 min, for $U_0 = 0.43$ m/s; $\psi = 4.88$. Values of porosities $\varepsilon = 0.3$; 0.4 and 0.6, from left to right.

The temperature profiles along the burner are shown in Figs. 7–10, at 5 min time intervals. In each figure, gas temperature is shown with a solid line, while solid temperature is depicted with a dashed line. Fig. 7 shows that a change in the mathematical model from a one-dimensional to a two-dimensional (right-hand side) caused an increment of about 5% in the temperature profile. Also, a faster combustion wave is calculated when a simplified one dimensional mathematical model is used, instead of the more complete two-dimensional model. The simplified 1D version of the mathematical model was used to validate the results obtained from the simulations with previously results obtained with the finite difference method by Foutko et al. [3]. Unsteady temperature distribution and combustion wave velocity results calculated with the 2D model were found to be in agreement with the experimental results reported by Foutko et al. [3].

The temperature profiles of either gas and solid, calculated with the 2D numerical simulation, are seen in Fig. 8

Table 4
Comparison between results of 1D and 2D models

Excess of air	Porosity	Inlet velocity (m/s)	Model	Gas maximum temperature (K)	Solid maximum temperature (K)	Combustion front velocity (m/s)
3	0.4	0.43	1D	1569.87	1417.39	9.583E−05
			2D	1640.45	1517.47	9.417E−05
4.88	0.4	0.43	1D	1404.44	1323.31	1.250E−04
			2D	1474.57	1413.95	1.258E−04
6	0.4	0.43	1D	1337.58	1275.48	1.408E−04
			2D	1413.48	1366.52	1.408E−04
4.88	0.3	0.43	1D	1424.87	1354.25	1.108E−04
			2D	1496.03	1448.81	1.092E−04
4.88	0.6	0.43	1D	1368.51	1258.09	1.858E−04
			2D	1437.38	1337.18	1.908E−04
4.88	0.4	0.3	1D	1333.79	1246.03	9.167E−05
			2D	1411.39	1337.21	8.917E−05
4.88	0.4	0.6	1D	1465.13	1394.07	1.750E−04
			2D	1513.48	1421.52	1.758E−04

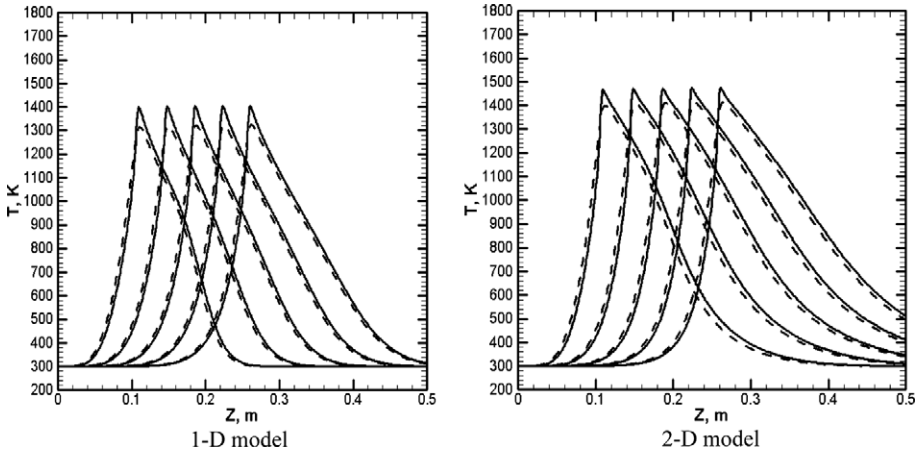

Fig. 7. Time variation of temperature profiles at time intervals of 5 min along the centerline, for $U_0 = 0.43$ m/s; $\varepsilon = 0.4$ and $\psi = 4.88$. Results for 1D model at left side and for 2D model on the right side.

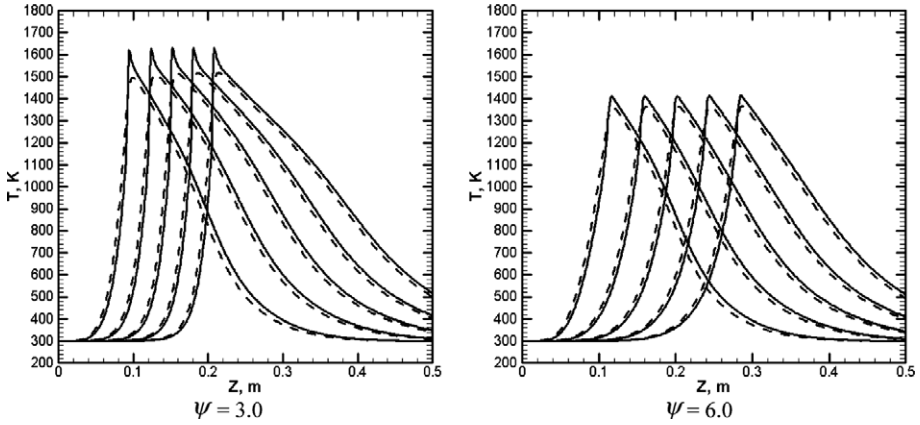

Fig. 8. Time evolution of temperature profiles at time intervals of 5 min along the centerline, for excess of air $\psi = 3.0$ on the left side and 6.0 on the right side ($U_0 = 0.43$ m/s; $\varepsilon = 0.4$).

to decrease by almost 18% when the excess air ratio increases from $\psi = 3.0$ to $\psi = 6.0$. Fig. 9 shows that a change in the porosity from $\varepsilon = 0.3$ to $\varepsilon = 0.6$ causes lower temperatures and a slower combustion wave, with a little bit larger temperature difference between gas and solid particles in the porous media.

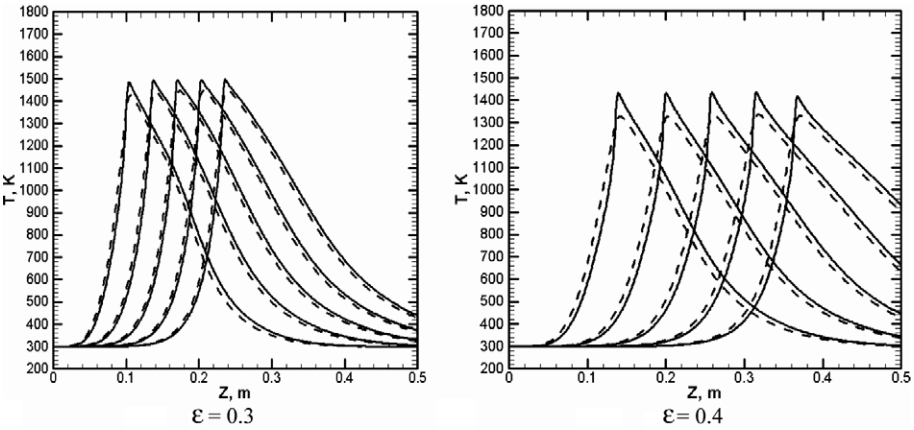

Fig. 9. Time evolution of temperature profiles at time intervals of 5 min along the centerline, for $\varepsilon = 0.3$ on left side and for $\varepsilon = 0.4$ on right side ($U_0 = 0.43$ m/s; $\psi = 4.88$).

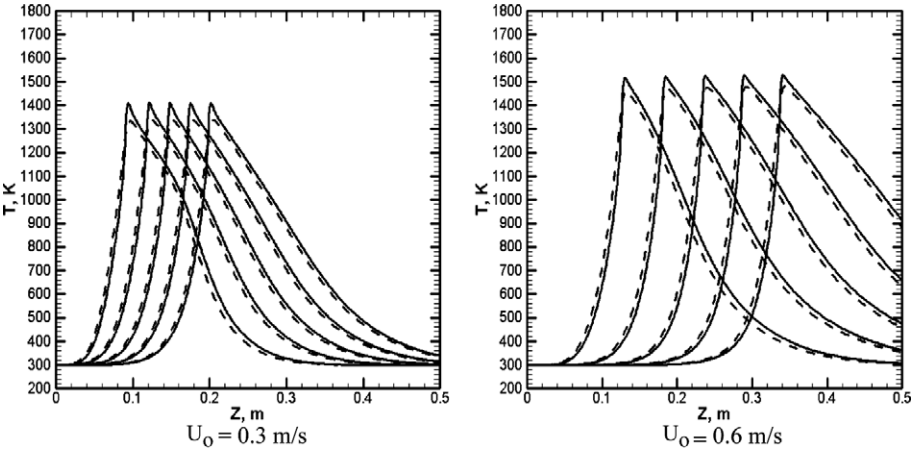

Fig. 10. Time evolution of temperature at time intervals of 5 min along the centerline, for $U_0 = 0.3$ m/s on left side and for $U_0 = 0.6$ m/s on right side ($\varepsilon = 0.4$ and $\psi = 4.88$).

An increment of the reactants inlet velocity from 0.3 m/s to 0.6 m/s caused an increment in the temperature profiles and a reduction in the combustion wave velocity, as it can be noticed in Fig. 10.

A comparison between the results obtained between the complete 2D mathematical model and a simplified 1D model is shown in Tables 4 and 5 for a maximum gas and solid temperature and for the wave combustion velocity. Relative deviations in the results obtained with the simplified 1D model can be as high as 7.1% for the maximum solid temperature; 5.7% for the maximum gas temperature and in the 0 to 1.74% range for the combustion wave velocity. In relative terms these differences seem to be not large, but considering that they are evaluated at the centerline, and that in absolute terms, specially the temperature could be over 1600 K, these differences become important, furthermore considering that they change in the radial direction.

Table 5
Relative differences between results of 1D and 2D models

Excess of air	Porosity	Inlet velocity (m/s)	Gas temperature (%)	Solid temperature (%)	Front velocity (%)
3	0.4	0.43	4.496	7.061	1.739
4.88	0.4	0.43	4.993	6.849	0.667
6	0.4	0.43	5.674	7.138	0.000
4.88	0.3	0.43	4.994	6.982	1.504
4.88	0.6	0.43	5.032	6.287	2.691
4.88	0.4	0.3	5.818	7.318	2.727
4.88	0.4	0.6	3.525	1.976	0.476

The temperature distribution calculated with the one-dimensional and two-dimensional mathematical models, when inlet velocity is 0.43 m/s, a porosity equals to 0.4 and a 4.88 excess of air, are shown in Fig. 11, at times of 5, 15 and 25 min. Main changes caused by the radial diffusion of heat, captured by the 2D model, are seen to be larger after the combustion zone.

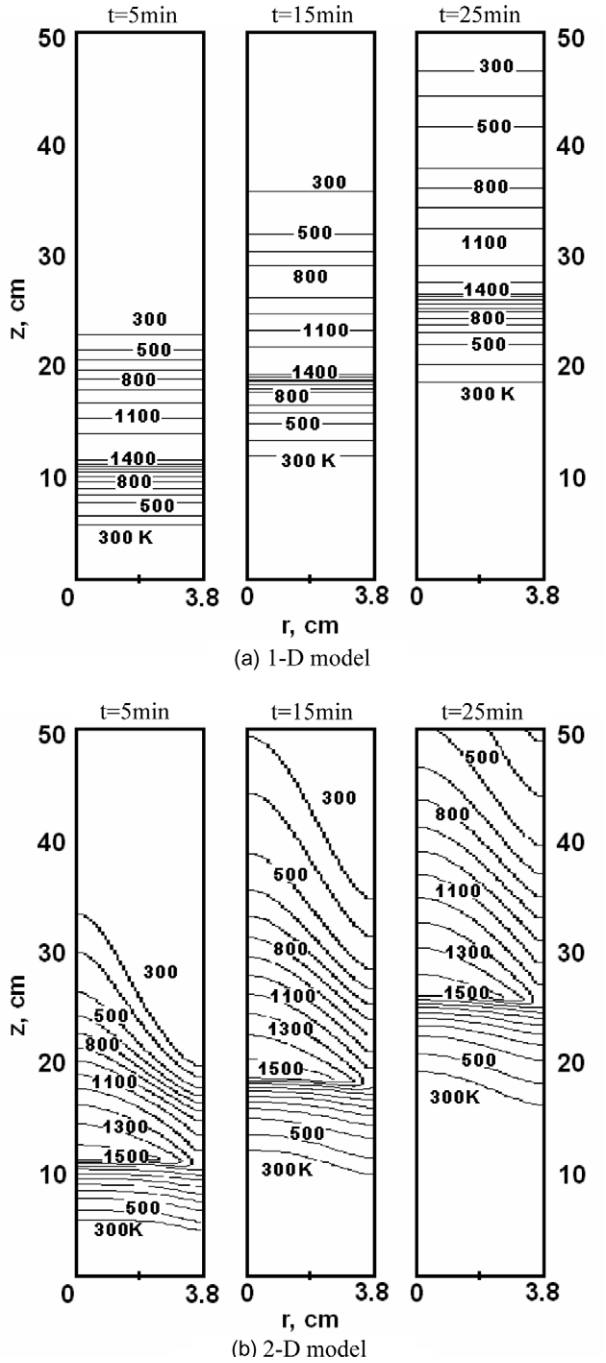

Fig. 11. Comparison of temperature distribution obtained at times equal to 5, 15 and 25 min, with 1D and 2D mathematical models.

Despite the fact that neither the effect of the hydrodynamic instability nor the channeling flow near the reactor wall can be captured with the mathematical model used, the unsteady two-dimensional temperature distribution and the wave combustion velocity can be predicted. These two dependent variables are very important for future technological applications. The use of the 2D model can be justified in the thermal design and location of heat exchangers in the porous media burner to withdraw the energy generated from the combustion process.

5. Conclusions

Convective heat transfer of methane with air in a cylindrical porous burner has been described in terms of a two-dimensional, two temperature mathematical model. Numerical simulations with the finite volume method have been accomplished with grids of 622×15 nodes, using dynamic time steps varying between 0.00001 and 1 s. The differences between the results obtained with the simplified 1D mathematical model have been found in order of 7.3% in temperatures and 2.7% in the combustion wave velocity, in comparisons with the results calculated from the 2D model. Radial heat conduction, calculated with the 2D model, accounted for larger differences in the temperature distribution after the combustion zone, when results were compared with those obtained by the simplified 1D model.

Acknowledgement

The authors acknowledge CONICYT-Chile for support received in the Fondecyt 1040148 project.

References

[1] S. Möβbauer, O. Pickenäcker, K. Pickenäcker, D. Trimis, Application of the Porous burner technology in energy and heat engineering, in: Proceedings of the Fifth International Conference on Technologies and Combustion for a Clean Environment, Lisbon, Portugal, 1999, pp. 519–523.
[2] D. Trimis, F. Durst, Combustion in a porous medium – advances and applications, Combust. Sci. Technol. 121 (1996) 153–168.
[3] S.I. Foutko, S. I. Shabunya, S.A. Zhdnadok, Superadiabatic combustion wave in a diluted methane–air mixture under filtration in a packed bed, in: Proceedings of the 26th International Symposium on Combustion/The Combustion Institute, Minsk, Belarus, 1996.
[4] S.A. Zhdanok, L.A. Kennedy, G. Koester, Superadiabatic combustion of methane–air mixtures under filtration in a packed bed, Combust. Flame 100 (1995) 221–231.
[5] V.S. Babkin, Pure Appl. Chem. 65 (1993) 335–344.
[6] J.R. Howell, M.J. Hall, J.L. Ellzey, Combustion of hydrocarbon fuels within porous inert media, Prog. Energy Combust. Sci. 22 (1996) 121–145.
[7] S.A. Zhdanok, K.V. Drobego, S.I. Futko, Flame localization inside axis-symmetric cylindrical and spherical porous media burners, Int. J. Heat Mass Transfer 43 (1997) 3469–3489.
[8] X. Zhou, G. Brenner, T. Weber, F. Durst, Finite-rate chemistry in modelling of two-dimensional jet premixed CH_4/air flame, Int. J. Heat Mass Transfer 42 (1999) 1757–1773.
[9] M.R. Henneke, J.L. Ellzey, Modeling of filtration combustion in a packed bed, Combust. Flame 117 (1999) 832–840.
[10] P.H. Bouma, P.H. de Goey, Premixed combustion on ceramic foam burners, Combust. Flame 119 (1999) 133–143.
[11] D.K. Min, H.D. Shin, Laminar premixed flame stabilized inside a honeycomb ceramic, Int. J. Heat Mass Transfer 34 (1991) 341–356.
[12] Y. Huang, C.Y.H. Chao, P. Cheng, Effects of preheating and operation conditions on combustion in a porous medium, Int. J. Heat Mass Transfer 45 (2002) 4315–4324.
[13] A.J. Barra, G. Diepvens, J.L. Ellzey, M.R. Henneke, Numerical study of the effects of materials properties on flame stabilization in a porous burner, Combust. Flame 134 (2003) 369–379.
[14] G. Brenner, K. Pickenäcker, O. Pickenäcker, D. Trimis, K. Wawrzinek, T. Weber, Numerical and experimental investigation of matrix-

stabilized methane/air combustion in porous inert media, Combust. Flame 123 (2000) 201–213.
[15] C.L. Hackert, J.L. Ellzey, O.A. Ezecoye, Combustion and heat transfer in model two-dimensional porous burners, Combust. Flame 116 (1999) 177–191.
[16] S.S. Minaev, S.I. Potytnyakov, V.A. Babkin, Combustion wave instability in the filtration combustion of gases, Combust. Explos. Shock Waves 30 (3) (1994) 306–310.
[17] K.V. Dobrego, I.M. Kozlov, V.I. Bubnovich, C.E. Rosas, Dynamics of filtration combustion front perturbation in the tubular porous media burner, Int. J. Heat Mass Transfer 46 (2003) 3279–3289.
[18] S.V. Patankar, Numerical Heat Transfer and Fluid Flow, Hemisphere, Washington, 1980.